LOCALLY ENRICHED QUADTREE GRID NUMERICAL MODEL FOR NEARSHORE CIRCULATION IN THE SURF ZONE

Koo-Yong Park

University of Oxford, Parks Road, Oxford, United Kingdom

Abstract: This paper describes an adaptive quadtree-based 2DH wave-current interaction model which is able to predict wave breaking, shoaling, refraction, diffraction, wave-current interaction, set-up and set-down, mixing processes (turbulent diffusion), bottom frictional effects, and movement of the land-water interface at the shoreline. The wave period- and depth-averaged governing equations are discretised explicitly by means of an Adams-Bashforth second-order finite difference technique on adaptive hierarchical staggered quadtree grids. Grid adaptation is achieved through seeding points distributed according to flow criteria (e.g. local current gradients). Results are presented for nearshore circulation at a sinusoidal beach. Enrichment permits refined modelling of important localised flow features

Key Words: nearshore circulation, quadtree grid, grid adaptation, surf zone

1. INTRODUCTION

An accurate description of nearshore hydrodynamics is very important, and much recent research effort has been directed towards numerical modeling of nearshore wave-current interaction, particularly using 2DH depth-averaged approaches on regular grids. Early numerical models (e.g. Noda, 1974) considered the wave climate and wave-induced current separately. In the 1980s it was recognized that these needed to be coupled, and so wave-current interaction models were developed that incorporated most of the important features of nearshore flows (e.g. Birkemeier and Dalrymple, 1976; Ebersole and Dalrymple, 1980; da Silva Lima, 1981; Yoo and O'Connor, 1986). The 2DH model is very useful for predicting horizontal circulation, rip currents and longshore currents, but is unable to evaluate either the undertow or the vertical profile of longshore currents, because the vertical distribution is averaged out by depth integration. Most 2DH models of wave-current interaction and storm surge flooding are based on fixed rectangular grids or uniform curvilinear boundary-fitted grids and therefore simulate the large-scale flow features on a structured grid system. It is inefficient computationally for the grid to be of uniformly high resolution throughout the entire domain; instead, adaptive local grid refinement offers a means of achieving the foregoing requirements.

A variety of robust, automatic and efficient non-uniform grid generation techniques are becoming available. Unstructured advancing front or Voronoi grids have been used for approximating complicated spatial geometries and can be readily adapted. However, grid quality checks can carry an expensive computational overhead, the nodal index system is extremely complicated, and nodal reordering is often required to make the solution matrix less sparse. An alternative approach considered herein is the application of hierarchical quadtree grids (Greaves and Borthwick, 1999) which maintain straightforward nodal connectivity through the tree structure, even though the grids may be highly non-uniform.

This paper describes a period- and depth-averaged 2DH wave-current interaction numerical model based on adaptive quadtree grids. The governing equations are discretised spatially using finite differences with all variables cell-centered, except the wave number and depth-averaged velocity components which are located on cell mid-faces. Time-dependent terms are integrated using an explicit Adams-Bashforth second-order scheme. Grid adaptation is achieved using seeding points located along shoreline boundaries and/or according to local wave amplitude and current gradient criteria. The model is verified by simulating nearshore circulation at a sinusoidal beach, and wave-induced currents at a multi-cusped beach.

2. QUADTREE GRID GENERATION

The quadtree algorithm has become increasingly applied in engineering for problems including image analysis (Samet, 1982) and finite element mesh generation (Greaves and Borthwick, 1999). Quadtree grid generation is undertaken within a unit square. The square is initially subdivided into four quadrants. Each cell is then subdivided into four smaller cells of equal sizes, and this process is recursively repeated until each cell meets certain boundary and flow criteria. The boundary criterion is that no cell should contain more than two seeding points, which are formed from the discretised boundary of the normalised flow domain. Flow criteria are problem specific, and may be that cell division depends on the magnitude of the wave amplitude or depth-averaged vorticity. This produces grids that are highly resolved in regions containing clusters of seeding points or rapidly varying flow features, but are sparse elsewhere.

It should be noted that quadtree grids have two disadvantages. First, the initial grid refinement can lead to adjacent cells of different sizes with hanging nodes on their interface edges. A hanging node occurs where the vertex of one cell lies on an edge of neighbour cell, and complicated approximations may be needed when discretising partial differential equations. Second, the boundary fit is not exact, although the mesh may be highly refined close to the boundary and so approximate it in a fractal sense.

For any given cell, its neighbors are identified by systematically searching the quadtree. A linked list data structure with recursion is used because of its efficiency in data accessing (Yiu *et al.*, 1996). Each link is built with pointers from the object cell to its parent cell and its subdivided cells. Hence every cell is identified by knowing the tree path relative to the root. The kth cell can be identified from

$$n_k = c_1 5^{m-1} + c_2 5^{m-2} + \ldots + c_{m-1} 5 + c_m \qquad (1)$$

where $c_1, \ldots, c_m$ are integer numbers and m is the cell's level. By dividing the identity number

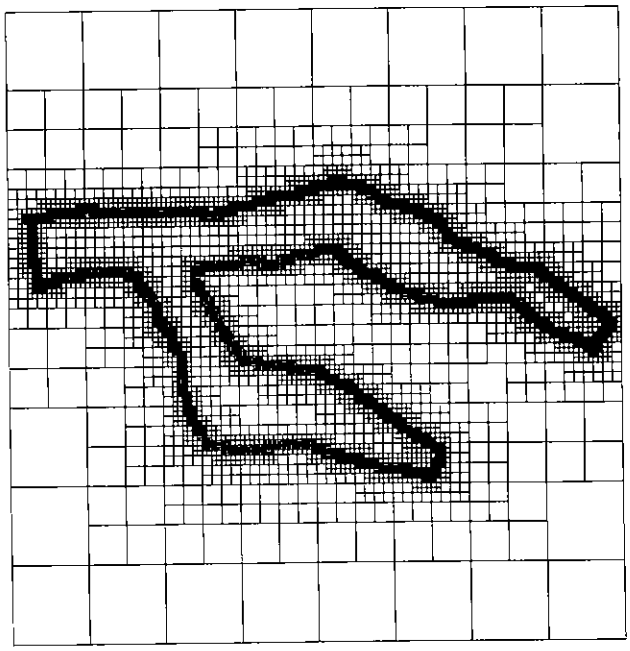

Fig. 1. An Example of 9-level Guadtree Mesh for a Bifurcating River Geometry

n_k by 5 repeatedly, the remainder 1, 2, 3, or 4 from the integer division indicate for cell's east, west, north or south. The identification number of the root cell is set to zero. Neighbor finding is achieved by first identifying the *Nearest Common Ancestor* (NCA) cell which is the smallest branching cell that is shared by the object cell and the neighbor under consideration. The nearest common ancestor may be a parent cell if the neighbor is a sister, a grandparent cell if the neighbor is a cousin, and so on. The identity numbers of the ancestral, sister, first cousin, second cousin, etc., cells are determined by simple integer manipulations of n_A from Eq. (1). The following example demonstrates the capability of the quadtree mesh generator to produce meshes for a complicated geometry. Fig. 1 depicts the quadtree grid generated about the boundary geometry of a bifurcating river.

3. GOVERNING EQUATIONS

The kinematic conservation equations of the wave-current interacted flow are shown as follows,

$$\frac{\partial K_i}{\partial t} + (Cg_i + U_j)\frac{\partial K_i}{\partial x_j} + S_{ij}\frac{\partial d}{\partial x_i} + K_j\frac{\partial U_i}{\partial x_i} - \frac{Cg}{2ka}\frac{\partial^3 a}{\partial x_i \partial x_j^2} = 0 \tag{2}$$

The radiation stress tensor may be written

$$S_{ij} = \frac{1}{2}\left[(1+\delta_{ij})(1+G)\frac{K_i}{K}\frac{K_j}{K} + G\delta_{ij}\right]\left(\frac{1}{2}\rho g a^2\right) \tag{3}$$

The depth-averaged continuity equation can be written as follows

$$\frac{\partial \eta}{\partial t}+\frac{\partial}{\partial x_i}(dU_i)=0 \tag{4}$$

The time-dependent, depth- and period-averaged momentum conservation equation can be expressed as

$$\frac{\partial U_i}{\partial t}+U_j\frac{\partial U_i}{\partial x_j}+\frac{1}{\rho d}\frac{\partial S_{ij}}{\partial x_j}+g\frac{\partial \eta}{\partial x_i}-\frac{\tau_{wi}-\tau_{bi}}{\rho d}-\frac{\partial}{\partial x_j}\left(\varepsilon_j\frac{\partial U_i}{\partial x_j}\right)=0 \tag{5}$$

After depth-integrating and period-averaging, the conservation of energy equation for the combined wave, current and turbulent flow becomes

$$\frac{\partial a}{\partial t}+\frac{1}{2a}\frac{\partial}{\partial x_i}\left\{(Cg_i+U_i)a^2\right\}+\frac{S_{ij}}{\rho ga}\frac{\partial U_j}{\partial x_i}+C^a a^2-\frac{1}{2}\frac{K_i}{K^2}\frac{\partial}{\partial x_j}\left(\varepsilon_j\frac{\partial}{\partial x_j}K_i a\right)=0 \tag{6}$$

The friction coefficient C^a is determined using Bijker's (1966) empirical formula. Thornton's algebraic formula yields a reasonable distribution of eddy viscosity in the surf zone where the wave breaking is dominant, and so it is used herein. Wave energy dissipation by wave breaking is modeled using US-CERC's (1984) empirical breaking criterion which effectively limits the ratio of wave height to water depth.

4. NUMERICAL MODEL

The quadtree grid can contain up to 49 possible cell arrangements, some of which are related through reflection or rotation. Here, the spatial discretisation was carried out on a uniform topology, with variables determined by linear interpolation where necessary, depending on the actual local cell configuration. The cell-centered

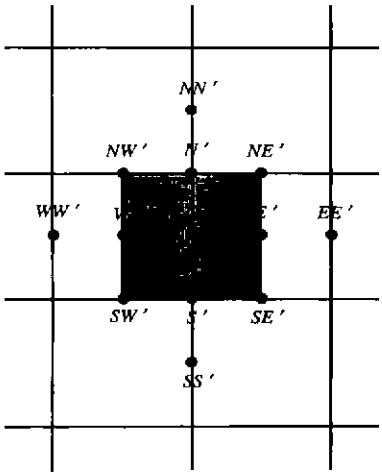

Fig. 2. Discretised Surface Elevation and Amplitude on Uniform Quadtree Grid

finite difference form of the continuity equation (4) is

$$\eta_C^{n+1}=\eta_C^n+\Delta t\left(\frac{3}{2}\frac{\partial \eta}{\partial t}\bigg|_C^n-\frac{1}{2}\frac{\partial \eta}{\partial t}\bigg|_C^{n-1}\right) \tag{7}$$

where

$$\frac{\partial \eta}{\partial t}\bigg|_C=-\Delta t\left[\frac{(Ud)_{I'}-(Ud)_{W'}}{\Delta x}+\frac{(Vd)_{N'}-(Vd)_{S'}}{\Delta y}\right]$$

in which Δt is the time step, Δx and Δy are the spatial grid increments, the subscripts refer to spatial position (see Fig. 2) and the superscripts n and n+1 indicate time levels.

The flux variables are determined by a linear interpolation. The discretised x-direction current momentum Eq. (5) at the quadtree cell face (see Fig. 3) is

$$U_{C'}^{n+1}=U_{C'}^n+\Delta t\left(\frac{3}{2}\frac{\partial U}{\partial t}\bigg|_{C'}^n-\frac{1}{2}\frac{\partial U}{\partial t}\bigg|_{C'}^{n-1}\right) \tag{8}$$

where

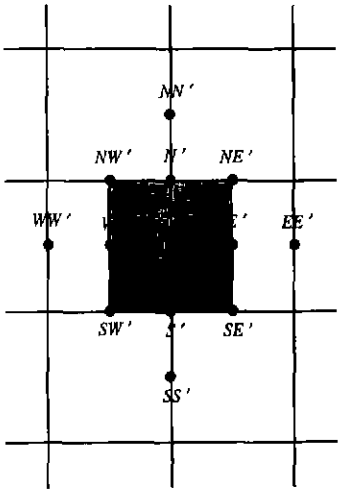

Fig. 3. Discretised x-direction Current and Wave Number on Uniform Quadtree Grid

$$\left.\frac{\partial U}{\partial t}\right|_{C'} = -\Delta t \left\{ U_{C'} \left.\frac{\partial U}{\partial x}\right|_{C'} + V_{C'} \left.\frac{\partial U}{\partial y}\right|_{C'} + \frac{1}{\rho\, d_{C'}} \left[\frac{S_{xE'} - S_{xW'}}{\Delta x} + \frac{S_{xN'} - S_{xS'}}{\Delta y} \right] + g \frac{\eta_{E'} - \eta_{W'}}{\Delta x} - \frac{\tau_{wxC'} - \tau_{bxC'}}{\rho\, d_{C'}} - \left(\varepsilon_{xC'} \frac{4U_{E'} - 8U_{C'} + 4U_{W'}}{\Delta x^2} + \varepsilon_{yC'} \frac{4U_{N'} - 8U_{C'} + 4U_{S'}}{\Delta y^2} \right) \right\}$$

First order upwind differences are used to discretise the spatial gradients, $\frac{\partial U}{\partial x}$ and $\frac{\partial U}{\partial y}$, in the nonlinear advection terms. In discretising the kinematic wave equation, the cartesian components of the wave number vector are denoted by P and Q. The upstream finite difference form of the x-direction kinematic wave Eq. (2) on the uniform quadtree grid depicted in Fig. 3 is given by

$$p_{C'}^{n+1} = p_{C'}^{n} + \Delta t \left(\frac{3}{2} \left.\frac{\partial p}{\partial t}\right|_{C'}^{n} - \frac{1}{2} \left.\frac{\partial p}{\partial t}\right|_{C'}^{n-1} \right) \tag{9}$$

where

$$\left.\frac{\partial p}{\partial t}\right|_{C'} = -\Delta t \left\{ R_{xC'}^{\vee} \left.\frac{\partial P}{\partial x}\right|_{C'} + R_{yC'}^{\vee} \left.\frac{\partial P}{\partial x}\right|_{C'} + P_{C'} \frac{U_{E'} - U_{W'}}{\Delta x} + Q_{C'} \frac{V_{E'} + V_{W'}}{\Delta x} + S_{hC'} \frac{d_{E'} - d_{W'}}{\Delta x} - \frac{G_{C'}^{K}}{2a_{C'}} \left[\left.\frac{\partial^3 a}{\partial x^3}\right|_{C'} + \frac{1}{\Delta x} \left(\frac{4a_{NE'} - 8a_{C'} + 4a_{SE'} - 4a_{NW'} + 8a_{W'} - 4a_{SW'}}{(\Delta y/2)^2} \right) \right] \right\}$$

The y-direction momentum equation and kinematic wave equation are discretised using the same procedure at the north face of the cell. The wave amplitude Eq. (6) is discretised about the cell-centre (Fig. 2) using the second order donor cell method, and becomes

$$a_C^{n+1} = a_C^{n} + \Delta t \left(\frac{3}{2} \left.\frac{\partial a}{\partial t}\right|_{C}^{n} - \frac{1}{2} \left.\frac{\partial a}{\partial t}\right|_{C}^{n-1} \right) \tag{10}$$

where

$$\left.\frac{\partial a}{\partial t}\right|_{C} = -\Delta t \left\{ \frac{1}{2a_C} \left(\frac{R_{xL'} a_R^2 - R_{xR'} a_L^2}{\Delta} + \frac{R_{yN'} a_U^2 - R_{yS'} a_B^2}{\Delta y} \right) + C_C^a a_C^n a_C^{n+1} - \frac{1}{2} \left(\varepsilon_{xC} \frac{4a_{E'} - 8a_C + 4a_{W'}}{\Delta x^2} + \varepsilon_{yC} \frac{4a_{N'} - 8a_C + 4a_{S'}}{\Delta y^2} \right) \right\} + \frac{1}{\rho\, g a_{C'}} \left[S_{xxC} \frac{U_{E'} - U_{W'}}{\Delta x} + S_{xyC} \left(\frac{U_{N'} - U_{S'}}{\Delta y} + \frac{V_{E'} - V_{W'}}{\Delta x} \right) + S_{yyC} \frac{V_{N'} - V_{S'}}{\Delta y} \right]$$

The radiation stresses are given on the uniform quadtree grid (see Fig. 2) as

$$S_{xxC} = \frac{\rho\, g}{4} (1 + G) \frac{P_{mx} Q_{my}}{k^2} a_C^2 \tag{11a}$$

$$S_{xxC} = \frac{\rho\, g}{4} \left[(1 + G) \frac{P_{mx}^2}{k^2} + G \right] a_C^2 \tag{11b}$$

$$S_{yyC} = \frac{\rho\, g}{4} \left[(1 + G) \frac{Q_{my}^2}{k^2} + G \right] a_C^2 \tag{11c}$$

Initially, U, V and η are set to zero, and the wave parameters (P, Q and a) are derived from Snell's law. No-flow conditions are applied to the offshore (inflow) boundary in the current field, as follows (see Fig. 4) giving $U_C = V_C =$

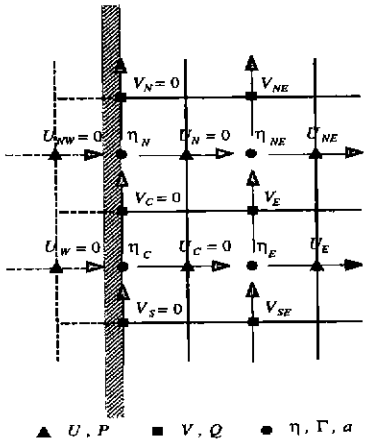

Fig. 4. Discretised Offshore Boundary Condition

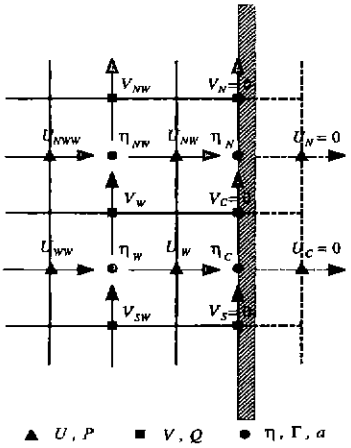

Fig. 5. Discretised Onshore Boundary Condition

$\Gamma_C = 0$ at $x = x_o$, where U and V refer to the x- and y-direction velocity components at the boundary, Γ represents all other variables at the boundary and x_o is the location of the offshore boundary. The surface elevation is given by $\eta_C = \eta_E$ at $x = x_o$. Offshore boundary values for the $P_C = K_E\cos 2_E$, and $Q_C = [(K+K_N)/2]$ sin $[(2+2_N)/2]$ where the non-subscripted variables are determined at the boundary, and H_o is the wave height in deep water.

At the onshore (nearshore) boundary in Fig. 5, the no-flow condition is $U_C = V_C = \Gamma_C = P_C = Q_C = a_C = 0$ and $\eta_C = \eta_W$ at $x = x_n$. Reflective lateral boundary conditions are given by $\Gamma_C = \Gamma_{NNN'}$, $\eta_C = \eta_{NN'}$, $a_C = a_{NN'}$, $U_C = U_{NN'}$ and $P_C = P_{NN'}$ if C is located on a south y-constant boundary, and $\Gamma_C = \Gamma_{SS'}$, $\eta_C = \eta_{SS'}$, $a_C = a_{SS'}$, $U_C = U_{SS'}$ and $P_C = P_{SS'}$ if C is located on a north y-constant boundary.

Boundary values of the y-direction velocity and wave number components are determined using the same procedure. Periodic boundary conditions (Fig. 6) are: $\phi_{R1} = \phi_{RN-2}$; $\phi_{R2} = \phi_{RN-1}$; and $\phi_{R3} = \phi_{RN}$ where N represents U, V, η, Γ, P, Q and a. A simple moving shoreline boundary scheme suggested by Birkemeier and Dalrymple

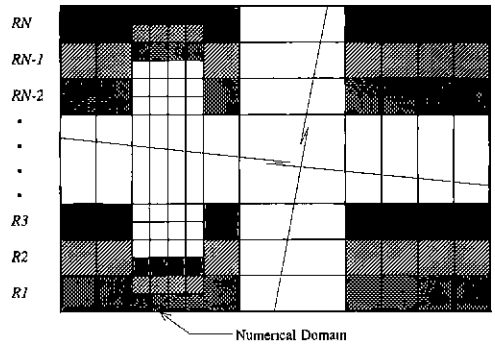

Fig. 6. Periodic Boundary Condition

(1976) is implemented in the present model. The time step is selected to be smaller than required by the 2-D Courant stability criterion. The separation factor k is calculated either by a Pade form explicit method ignoring current effects (Hunt, 1979). The whole process is repeated each time step until the flow converges to steady-state.

5. RESULTS

In this verification test, the numerical model is used to simulate nearshore circulation, due to a combination of longshore and rip currents at a sinusoidal beach. In 1981, da Silva Lima obtained experimental data on nearshore cir-

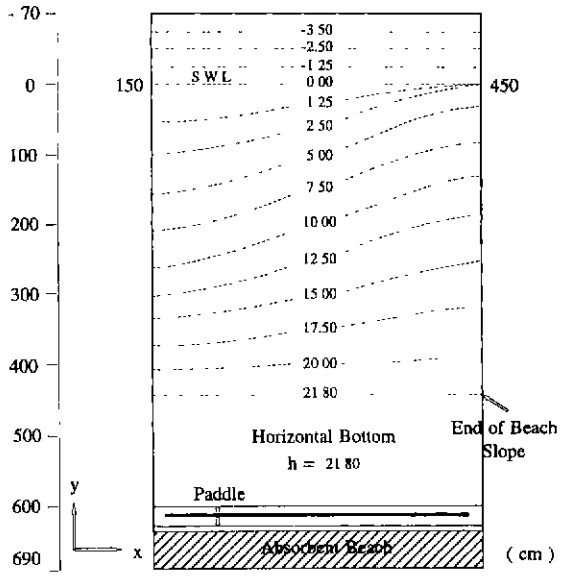

Fig. 7. Water Depth Contours for Half-sinusoidal Beach by da Silva Lima (1981)

culation at a half-sinusoidal beach in a wave basin 7.6 m long, 3 m wide and 0.218 m offshore depth at the wave paddle (see Fig. 7).

Fig. 8 presents the measured period-averaged current pattern for normal incidence offshore waves of height H_o = 0.0618 m and period T = 0.76 s at normal incidence to the shoreline of the plane beach.

He determined current velocities by tracking floats which he designed to move at mid-depth. The computations are first performed on a 32 × 32 uniform mesh covering a domain of dimensions of 6.4 m in the x-direction and 3.0968 m in the y-direction, with grid spacings Δx = 0.2 m and Δy = 0.096775 m. To avoid numerical instability emanating from the discretised nonlinear advection terms, a time step of 0.005 s was used, well below the Courant limit, and the

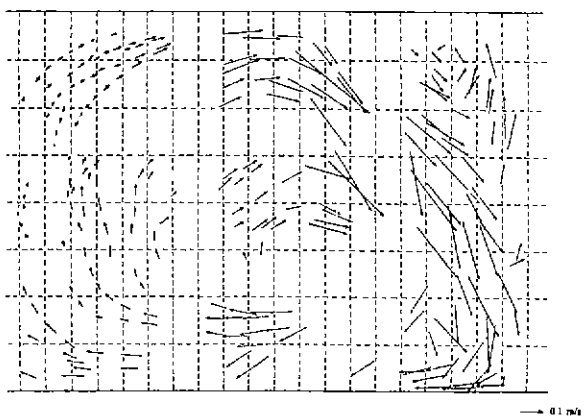

Fig. 8. Steady State Nearshore Current Pattern for da Silva Lima's (1981) Beach: Uniform Grid

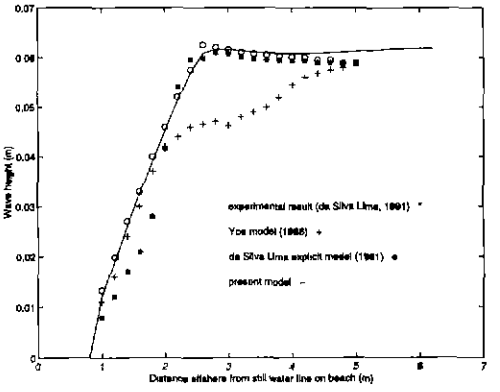

Fig. 9. Wave Height Profiles for da Silva Lima's (1981) Beach Along the Centre Line of Numerical Domain

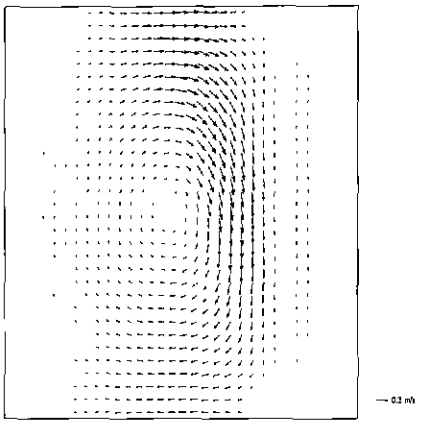

Fig. 10. Steady State Nearshore Current Pattern for da Silva Lima's Beach: Uniform Grid

simulation undertaken until t = 100 s, with steady-state reached at about 50 s. The dimensionless constant in the Thornton formula, M_T, and the bottom friction coefficient C_f are ramped down linearly from relatively high initial values to M_T = 1.0 and C_f = 0.03, to help retain computational stability when wave-current interaction is switched on. The seiching period, T_s, and time before permitting full wave-current interaction to occur, T_{cur}, are both set to 11 s. For wave breaking, US-CERC's criterion is used. Reflective side wall conditions are applied at the solid lateral boundaries. A minimum depth criterion of 0.001 m prevents overflow errors in determining the wave number during the computation. Fig. 9 shows the wave height distribution with distance from the beach.

The results demonstrate that the present scheme gives predictions in close agreement with da Silva Lima's experimental data, whereas Yoo and O'Connor's (1986) numerical model somewhat under-estimates the wave heights in the breaker region. As would be expected, the wave heights rapidly decrease to zero onshore after breaking. This rapid loss in height of the broken waves may promote strong radiation stresses which in turn may create large and possibly unstable currents. The computed nearshore current pattern is shown in Fig. 10 at time t = 100 s.

The anticlockwise secondary gyre in the shallowest depths near the beach is slightly less strong than the experimental measurements. This may be due to numerical dissipation caused by the use of first order upwinding for the nonlinear convective terms in the momentum equation. It may also be linked to empirical inaccuracies in the simple wetting and drying algorithm which is unable to handle the final set-up grid point (inshore direction) perfectly. However the wave-induced current patterns results do show good overall agreement with the experimental data produced by da Silva Lima (see Fig. 8) and numerical results of da Silva Lima (1981), Yoo and O'Connor (1986), Borthwick and Joynes (1989), and Dong and Anastasiou (1991).

In a separate test, the initial uniform mesh was adapted according to the following cell circulation parameter,

$$\Lambda = \left(\frac{\partial V}{\partial x} - \frac{\partial U}{\partial y} \right) \Delta x \, \Delta y \qquad (12)$$

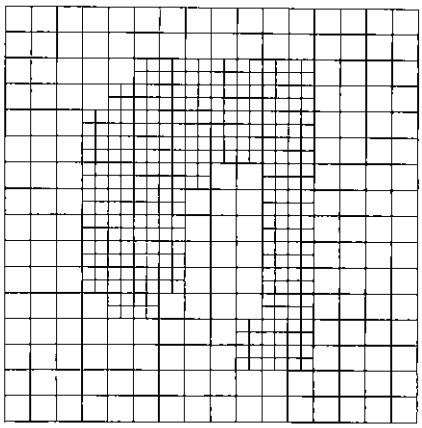

Fig. 11. Adapted Mesh According to the Parameter Starting from a 16 × 16 Uniform Mesh

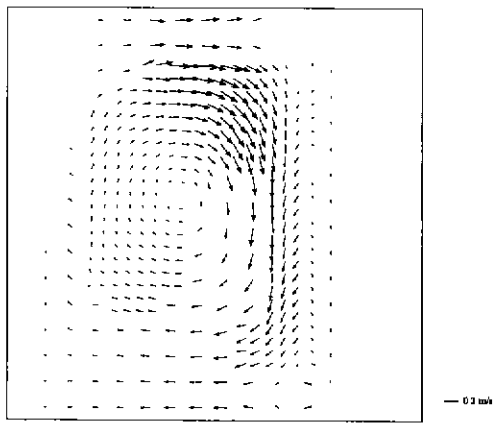

Fig. 12. Period-Averaged Current Velo City-Vectorsn the Adapted Mesh

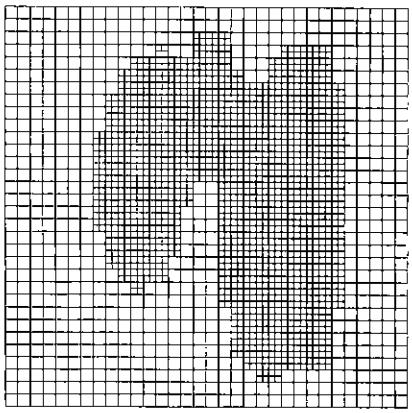

Fig. 13. Adapted Mesh According to the Circulation Parameter Starting a 32 × 32 Uniform Mesh

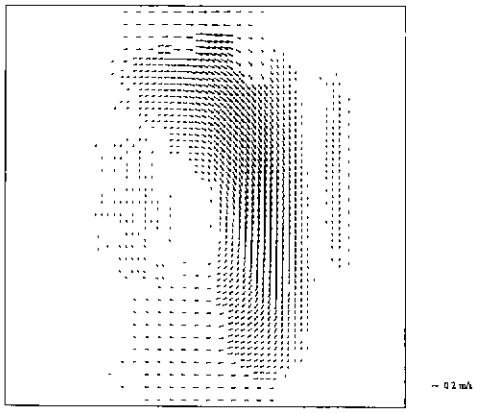

Fig. 14. Period-Averaged Current Velocity-Vectors on the Adapted Mesh from

and the induced-current then computed on the refined mesh until t = 100 s. All cells where $7 > 7_{max} / 7.0$ (in which 7_{max} is the maximum value of 7 within the computational domain) were subdivided, and the grid regularized. Figs. 11 and 12 show the adapted mesh and nearshore circulation pattern obtained for an initial uniform 16 × 16 mesh. The corresponding results commencing with a uniform 32 × 32 mesh are presented in Figs. 13 and 14.

The computed flow patterns are almost the same for the previous regular grid results, and are in close agreement again with da Silva's experimental data. This indicates that the present model is capable of high resolution in regions of high current shear.

6. CONCLUSIONS

This paper has presented an adaptive quadtree grid based numerical model of wave-current interaction. The quadtree grid generator is fast, fully-automatic, reliable, and computationally

efficient due to a linked-list technique which optimizes grid information handling. The method is ideally suited to mesh adaptivity, with local enrichment and coarsening determined by flow, bed topography or boundary criteria. It offers a sensible means of meshing coastal domains containing complicated shoreline geometries. A drawback of quadtree gridding is that the boundary fit is only approximate, though this is counteracted to some extent by the inherent high resolution of the grid at discretised boundaries.

The nearshore circulation was simulated at an idealized half-sinusoidal beach. The model predictions were compared with experimental data from da Silva Lima (1981). The predictions were convergent and achieved steady-state with periodic boundary conditions and incorporation of the non-linear advection term in the discretised momentum equation. The profile of wave height was very accurately predicted in comparison with experimental data. The nearshore circulation pattern is also closely in agreement with the experimental data. The anticlockwise secondary gyre near the beach is slightly less strong than obtained experimentally because of the simple wetting and dry algorithm. The quadtree grid was then successfully adapted according to the circulation parameter, starting from a 32×32 uniform mesh. The predicted wave-induced circulation pattern on the enriched quadtree mesh is in very good agreement with the results from the uniform mesh. These results indicate that the potential of model for evaluating refined surf-zone hydrodynamics in complicated coastal geometries.

ACKNOWLEDGEMENTS

This work was supported by the Hyundai Engineering and Construction Co. Ltd. The U.K. Engineering and Physical Sciences Research Council funded the multi-cusped beach studies through grant GR/K04125.

REFERENCES

Birkemeier, W.A. and Dalrymple, R.A. (1976) "Nearshore water-circulation induced by wind and waves", *Proc. of the Sym. on Modelling Tech.*, ASCE, pp.1062-1081.

Borthwick, A.G.L., Foote, Y.L.M. and Ridehalgh, A. (1997) "Nearshore measurements at a cusped beach in the U.K. Coastal Research Facility", *Coastal Dynamics '97*, Plymouth, pp.953-962.

da Silva Lima, S.S.L. (1981) "Wave-induced Nearshore Currents", Ph.D. Thesis, Department of Civil Engineering, University of Liverpool.

Ebersole, B.A. and Dalrymple, R.A. (1980) "Numerical modelling of nearshore circulation", *Proc. 17th Conf. on Coastal Eng*, ASCE, 4, 2710-2725.

Greaves, D.M., and Borthwick, A.G.L. (1999) "Hierarchical tree-based finite element mesh generation", *Int. J. for Numer. Methods in Engineering*, 45, pp.447-471.

Hunt, J.N. (1979), "Direct solution of wave dispersion equation", *Journal of Waterways, Ports, Coastal Ocean Engineering*, ASCE, Vol. 105, No. WW4, pp. 457-459.

Komar, P.D. (1998) *Beach Processes and Sedimentation*, 2nd Ed., Prentice Hall, New Jersey.

Noda, E.K. (1974) "Wave-induced nearshore circulation", *J. Geophys. Res.*, 79(27), pp.4097-4106.

Samet, H. (1982) *Neighbour Finding Techniques for Images Represented by Quadtrees Data Structures*, Computer Graphics and Image Processing, Vol. 18, pp. 37-57.

Shi, F., Sun, W. and Wei, G. (1997) "A WDM method on a generalized curvilinear grid for calculation of storm surge flooding", *Applied Ocean Res.*, Vol. 19, pp. 275-282.

US-CERC (1984), *Shore Protection Manual,* Coastal Engineering Research Center, Corps of Engineers, Vol. 1,2, Government Printing Office.

Yiu, K.F.C., Greaves, D.M., Cruz, S, Saalehi, A. and Borthwick, A.G.L. (1996) "Quadtree grid generation: Information handling, boundary fitting and CFD applications", *Computer & Fluids*, 25(8), pp.759-769.

Yoo, D., and O'Connor, B.A. (1986) "Mathematical modelling of wave-induced nearshore circulations", *Proc. 20th International Conference on Coastal Engineering*, ASCE, pp.1667-1681.

D.Phil Research Student, University of Oxford, Parks Road, Oxford, United Kingdom, OX1 3PJ

Present Address : Hyundai Engineering and Construction Com., Ltd., Kye-Dong 140-2, Chongro-Gu, Seoul

(Received March 16, 2000; accepted April 10, 2000)